



# SARS-CoV-2 Virion Stabilization by Zn Binding

Silvia Morante<sup>1,2\*</sup>, Giovanni La Penna<sup>2,3</sup>, Giancarlo Rossi<sup>1,2,4</sup> and Francesco Stellato<sup>1,2</sup>

<sup>1</sup> Dipartimento di Fisica, Università di Roma "Tor Vergata", Rome, Italy, <sup>2</sup> INFN, Sezione di Roma Tor Vergata, Rome, Italy, <sup>3</sup> CNR, Institute of Chemistry of Organometallic Compounds, Firenze, Italy, <sup>4</sup> Centro Fermi - Museo Storico della Fisica e Centro Studi e Ricerche "Enrico Fermi", Rome, Italy

Zinc plays a crucial role in the process of virion maturation inside the host cell. The accessory Cys-rich proteins expressed in SARS-CoV-2 by genes ORF7a and ORF8 are likely involved in zinc binding and in interactions with cellular antigens activated by extensive disulfide bonds. In this report we provide a proof of concept for the feasibility of a structural study of orf7a and orf8 proteins. A conceivable hypothesis is that lack of cellular zinc, or substitution thereof, might lead to a significant slowing down of viral maturation.

**Keywords:** SARS-CoV-2, Zn binding, molecular dynamics computer simulation, zinc finger, tetherin/Bst2, orf7a and orf8 proteins

## OPEN ACCESS

### Edited by:

Mario Nicodemi,  
University of Naples Federico II, Italy

### Reviewed by:

Qin Xu,  
Shanghai Jiao Tong University, China  
Vered Wineman-Fisher,  
University of South Florida,  
United States

### \*Correspondence:

Silvia Morante  
silvia.morante@roma2.infn.it

### Specialty section:

This article was submitted to  
Biophysics,  
a section of the journal  
Frontiers in Molecular Biosciences

**Received:** 23 May 2020

**Accepted:** 07 August 2020

**Published:** 17 September 2020

### Citation:

Morante S, La Penna G, Rossi G and  
Stellato F (2020) SARS-CoV-2 Virion  
Stabilization by Zn Binding.  
*Front. Mol. Biosci.* 7:222.  
doi: 10.3389/fmolb.2020.00222

## 1. INTRODUCTION

The SARS-CoV-2 open reading frames ORF7a and ORF8 code for virion non-structural, called accessory (Coffin et al., 1997), proteins of yet unknown function (orf7a and orf8, respectively, hereafter). The protein orf7a is common to all SARS-CoV type coronaviruses and highly conserved (Wu A. et al., 2020), while orf8 is remarkably different from proteins coded by genes ORF8 and ORF8b of human SARS-CoV (Xu et al., 2020).

The orf7a protein of SARS-CoV-1 has been shown to interact with several host proteins (Vasilenko et al., 2010). An analogous situation occurs in the case of the very similar SARS-CoV-2 orf7a protein (Gordon et al., 2020). The most supported hypothesis proposed for orf7a protein function is the interference with virion budding tethering (Bonifacino and Glick, 2004) operated by cellular antigens (Taylor et al., 2015). Indeed, orf7a is expressed in the host cell to inhibit the intracellular (at endoplasmic membrane) process of virion immobilization before and after virion vesiculation. On the basis of structural similarities (Swiecki et al., 2013) we argue that also protein orf8 can be involved in the same inhibition process, strengthening the inhibition of virion immobilization. This conjecture is in agreement with Gordon et al. (2020) where it is suggested that orf8 plays a role in vesicle trafficking and in endoplasmic reticulum protein quality control, thus favoring the reconfiguration of ER/Golgi trafficking during coronavirus infection.

Virion tethering is mainly due to proteins of the tetherin family, also known as bone marrow stromal antigen 2 (BST2) or cluster of differentiation 317 (CD317). BST2 is expressed in many cells in the interferon-dependent antiviral response pathway. The mechanism of tethering involves tetherin protein dimerization via formation of extended disulfide bonds within the coiled coil region (Le Tortorec et al., 2011). This step is known to be strongly influenced by divalent cations involved in Cys binding. Among these ions, the most available in cells is Zn<sup>2+</sup>.

A timely computational search for therapeutic targets of SARS-CoV-2 found the orf7a-BST2 complex as a potential target to be addressed with structural studies (Wu C. et al., 2020).

The orf7a and orf8 protein sequences (both 121 amino acids long) hint at a high Zn binding propensity, as they display 6 Cys/3 His and 7 Cys/4 His side-chains, respectively, with motifs that are able to bind Zn, thus forming multiple zinc finger (ZF) domains. The relevance of Zn in the viral replication process has been widely investigated (Chaturvedi and Shrivastava, 2005; Chasapis, 2018) and, indeed, two ZF domains have been discovered in the nucleocapsid protein of HIV-1 (Ncp7) (Morellet et al., 1998; Guo et al., 2000). Two such similar Zn domains have been also identified (Kirchdoerfer and Ward, 2019) along the highly conserved, within the SARS-CoV family (Xu et al., 2020), nsp12 polymerase.

## 2. METHOD AND RESULTS

The pivotal role of Zn in SARS-CoV replication has been demonstrated by inhibition of RNA polymerase activity both *in vitro* and in cell culture (te Velthuis et al., 2010).

Comparing with the well assessed ZF domains of Ncp7 CX<sub>2</sub>CX<sub>4</sub>HX<sub>4</sub>C (located from aa 15 to aa 28 and from aa 36 to aa 49), one identifies the similar CX<sub>3</sub>HX<sub>3</sub>C and CX<sub>8</sub>CX<sub>5</sub>H motifs in orf7a (located from aa 15 to aa 23 and from aa 56 to aa 73, respectively) and the HX<sub>2</sub>CX<sub>4</sub>CX<sub>2</sub>H motif in orf8 (located from aa 17 to aa 28). The patterns of these motifs are shown in **Figure 1**.

UNIPROT ([https://www.uniprot.org/help/zn\\_fing](https://www.uniprot.org/help/zn_fing)) reports a large variety of ZF domains among which also the Cys-rich patterns of orf7a and orf8 can be accommodated.

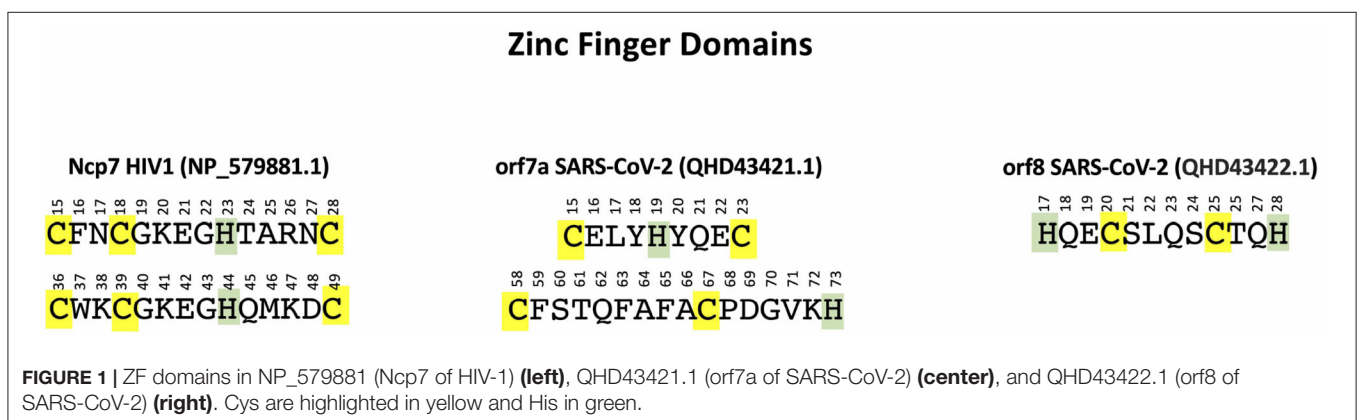
From a structural point of view it is not difficult to come up with a plausible protein structure capable of hosting a Zn<sup>2+</sup> ion. Focusing on orf7a as an example, one can proceed to construct such structures by first building an atomistic model of the protein in a random coil configuration. After simulating self-avoiding random walks (La Penna et al., 2004; Furlan et al., 2008) of the chain in vacuum by randomly changing the dihedral angles (not involving H atoms) of all residues (except  $\Phi$  in Pro), for a total of 445 dihedral angles, we proceeded by monitoring along the trajectory the distance  $d$  between pairs of S $\gamma$ (Cys)-S $\gamma$ (Cys) atoms,  $d(CC)$ , and S $\gamma$ (Cys)-N $\epsilon$ (His) atoms,  $d(CH)$ . All His side-chains are neutral and protonated at N $\delta$ . We collected a trajectory of 400 random configurations, with consecutive configurations

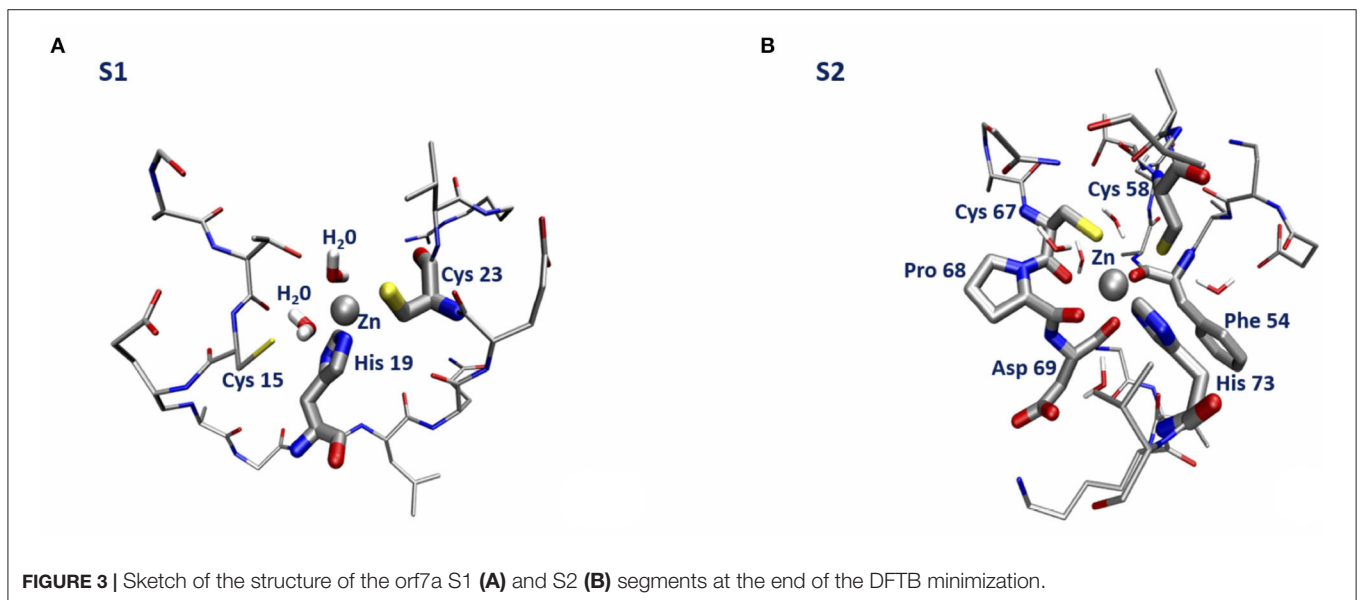
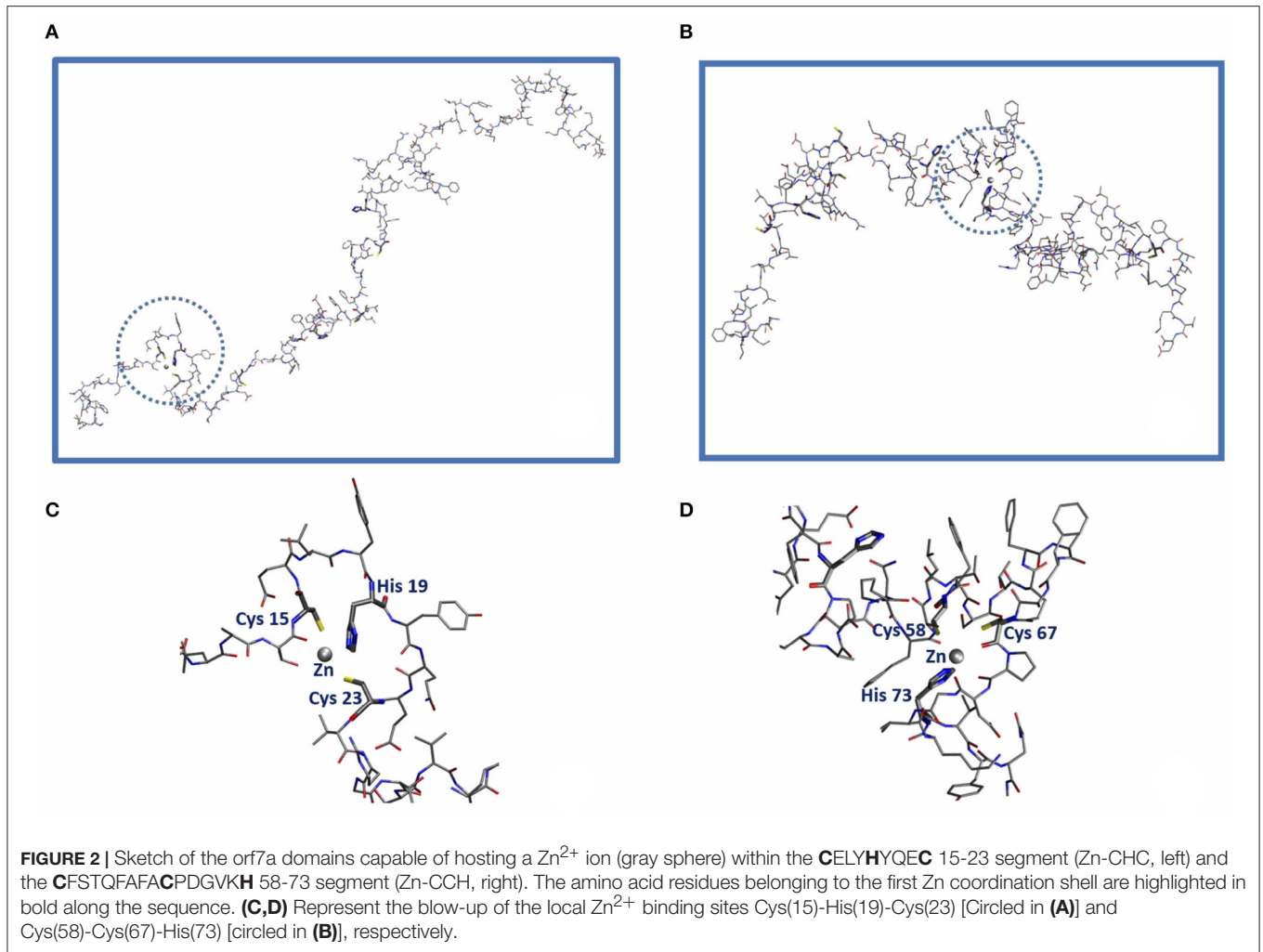
separated by 500 attempted torsional moves. Acceptance ratio was about 0.5. Two chain configurations where three among all of the possible  $d(CC)$  and  $d(CH)$  distances are smaller than 1.2 nm were selected. This condition was found to be satisfied by the triplets Cys(15)...His(19)...Cys(23) in one case and Cys(58)...Cys(67)...His(73) in a second case. Zn<sup>2+</sup> ions were then inserted at the geometric center of each of the two selected triplets of atoms. A cationic dummy atom model for Zn (Pang, 2001) and the PARM14 Amber force-field (Maier et al., 2015) for the protein were used. We took a distance cut-off for non-bonding interactions of 0.5 nm, with Coulomb interactions shifted and damped to achieve local neutralization (Wolf et al., 1999). Starting from the selected configurations, we relaxed the systems by classical molecular dynamics (MD). At the beginning, harmonic forces with  $k = 10$  kcal/mol/Å<sup>2</sup> were added to bring the distances between Zn and the three atoms [S $\gamma$ (Cys(15)), N $\epsilon$ (His(19)), S $\gamma$ (Cys(23))] in the first case (site Zn-CHC) and [S $\gamma$ (Cys(58)), S $\gamma$ (Cys(67)), N $\epsilon$ (His(73))] in the second (site Zn-CCH) from the initial values down to 2.5 Å in 10 ps. The final configurations of sites Zn-CHC (segment S1: 15–23) and Zn-CCH (segment S2: 58–73) are displayed in **Figure 3**, left and right panels, respectively. All calculations were performed with the LAMMPS code (Plimpton, 1995).

We interpret the fact that we have been able to get Zn-CHC and Zn-CCH stable configurations already with very simple classical simulation techniques, as a strong indication of the high propensity to give raise to ZF domains as soon as the occurrence frequency of Cys and His along the protein (or in its environment) is sufficiently high.

### 2.1. Refining the Zn Binding Sites

In the previous section by means of empirical non-polarizable force fields we have built candidates Zn binding sites for the orf7a protein of SARS-CoV-2. A more realistic description of Zn-protein interactions, especially when Zn-S bonds occur, requires polarizable or reactive force fields (Zhang et al., 2012; Li and Merz, 2017). Semiempirical quantum mechanics methods, like those driven by the density-functional tight-binding approximated (DFTB) hamiltonian (Elstner et al., 1998), include polarization and charge transfer in the calculation of atomic forces and allow energy minimization of systems of thousands



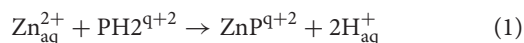


of atoms within periodic boundary conditions (Hourahine et al., 2020). In this subsection we explore the energy profile around the previously selected configurations, using a DFTB hamiltonian.

Since the candidate Zn binding sites displayed in **Figure 2** involve a limited protein region, we built model configurations of the systems of interest by truncating the protein around the ZF domains involved in Zn binding. We choose for the Cys(15)-His(19)-Cys(23) and Cys(58)-Cys(67)-His(73) binding sites the Ala<sub>13</sub>...Gly<sub>26</sub> and the Asp<sub>51</sub>...Val<sub>74</sub> segments, called for short S1 and S2, respectively, in the following. The N- and C-termini of the segments were capped with acetyl and N-methyl groups, respectively. Cys binding side-chains were assumed as deprotonated according to NMR measurements of ZF domains (Tochio et al., 2015).

For each one of the two segments we constructed a simulation box by inserting the corresponding amino acids together with Zn into an orthorhombic cell whose volume is minimized by rotating the protein segments. The cell was then filled of TIP3P water molecules (Jorgensen et al., 1983) with the help of the “solvate” utility of VMD (Humphrey et al., 1996). At this point the energy of the system was first minimized for as long as 2000 conjugate gradient (CG) steps by moving water molecules and capping groups only. The same force field as the one we used in the previous classical self-avoiding random walk simulation was employed here. The final configurations were then used as the initial configurations in the CG energy minimization performed with the DFTB hamiltonian. The DFTB+ code (Hourahine et al., 2020) was used with the znorg-0-1 parametrization (Moreira et al., 2009). The energy is assumed to be in a minimum when the maximal force component was lower than 0.01 Ha/Bohr. Convergence was achieved within 150 steps in all cases.

In order to estimate the formation energy of the Zn binding sites in the minimized configurations we obtained, we compare the former with two new systems that are obtained by exchanging the position of the Zn ion with that of the O of a water molecule lying far from the protein side-chains, upon transferring the entire water molecule where the Zn was located. After the exchange, the Cys side-chains turn out to be protonated. The exchange of Zn with a water molecule is represented by the chemical reaction



where PH<sub>2</sub> is the protein segment with protonated Cys side-chains (when not bound to Zn), ZnP represents the complex formed by Zn and the deprotonated protein.

The charge *q* of the protein is  $-3$  and  $-2$  for the S1 and S2 segments, respectively. The energy of each complex was therefore corrected for the Makov–Payne term (Makov and Payne, 1995), to take into account the difference in the cell net charge from the initial to the final state of the reaction (1).

The uncorrected energy of reactants is computed as the lowest energy of the system with Zn exchanged with a bulk water molecule. The energy of the product in reaction (1), ZnP, is that of the complex in the box. The energy of hydrated proton is, as usual, taken from experiments (Raffa et al., 2007). After correcting for the Makov–Payne term (Makov and Payne, 1995)

**TABLE 1** | Energy variation ( $\Delta E$ , kJ/mol) between the initial and final minimized configurations in the reaction (1) for our models of the binding sites S1: Cys(15)-His(19)-Cys(23) and S2: Cys(58)-Cys(67)-His(73).

Segment	$\Delta E$
S1	−376
S2	−1,242

**TABLE 2** | Geometry of the first Zn coordination shell of the orf7a S2 segment at the end of the DFTB minimization.

Residue	Atom	Distance [Å]
Phe 54	O	2.30
Cys 58	S	2.78
Cys 67	S	2.38
Pro 68	O	2.32
Asp 69	O	2.23
His 73	N	2.00

*We report atoms lying within 3 Å from the metal.*

**TABLE 3** | Geometry of the first Zn coordination shell of the orf7a S1 segment at the end of the DFTB minimization.

Residue	Atom	Distance [Å]
His 19	N	1.97
Cys 23	S	2.29
Wat	O	1.99
Wat	O	2.04

*We report atoms lying within 3 Å from the metal.*

one gets the numbers reported in **Table 1**. We stress that both numbers are negative, meaning that Zn is bound to the ZF domains of the segments S1 and S2.

The lowest energy configurations obtained in the DFTB approximation are displayed in **Figures 3A,B**. The coordination geometry around the Zn binding sites at the end of the DFTB minimization are reported in **Tables 2, 3** where the distances of the atoms lying within 3 Å from the metal are reported. It is worth noticing that approximately the arrangement of the first shell Zn ligands is tetrahedral in the case of S1 and octahedral in the case of S2.

We end with a few remarks. First of all, we observe that the mechanical constraints acting within the bent protein regions are not sufficient to break the Zn bond. Secondly, we see that, while in the S1 Zn binding site S $\gamma$ (Cys 15) is replaced by a water molecule (see **Figure 3A**), the structure of the S2 Zn binding site is remarkably stable, as a consequence of the small probability for a water molecule to enter the first Zn coordination shell. The structural stability of the Zn bonds is ensured by presence of 2–3 carbonyl groups that keep Zn bound to the two S $\gamma$  atoms on the opposite side, with the His side-chain unperturbed by the protein small relaxation. Finally, we stress that the formation energy of the Zn bound complexes is dominated by the negative empirical contribution of the extraction of two protons into bulk water.

### 3. DISCUSSION

With the help of classical MD simulations complemented with semiempirical quantum mechanics methods we have provided convincing evidence for the key role played by  $Zn^{2+}$  in stabilizing the orf7a (and possibly also) orf8 protein. Our working assumption is that orf7a (and/or orf8) can make  $Zn^{2+}$  available to BST2. The stability of Zn-S bonds, with S belonging to reduced sulfide groups, can in turn favor the breaking of some of the disulphide bridges of the folded BST2 tetherin, allowing the formation of inactivated orf7a/BST2 (and/or orf8/BST2) complexes with inhibition of the BST2 antiviral activity.

Based on the above considerations, we would like to argue that, although the affinity of Zn for the ZF domains is large (and larger than for other divalent cations of similar size available in cells, like  $Mg^{2+}$ ), one might think of displacing  $Zn^{2+}$  upon altering concentration in the host cells by temporary Zn deprivation and Mg augmentation. Indeed, situations have been identified in which, depending on the specific amino acids forming the metal coordination site, proteins can preferentially bind  $Mg^{2+}$  over  $Zn^{2+}$  (Gati et al., 2017).

Thus, cellular Zn deprivation, with Zn replacement by Mg and/or specific drugs based on Ag(I) or Au(I) (Kluska et al., 2020), might result in a significant slowing down of viral replication, owing to the inhibition of orf7a/BST2 and orf8/BST2 complexes formation. Circumstantial support for this hypothesis comes from the well-known, important role played by Zn in inflammation (Gammoh and Rink, 2017).

According to the scenario we have described, we are engaged in the long-term project of producing atomistic models of the orf7a/BST2 and orf8/BST2 systems, that can serve as reliable

templates in the analysis of the forthcoming experiments aimed at unveiling the formation pathways and the detailed structure of these complexes.

The comparison to known related structures, i.e., the N-terminal ectodomain of orf7a of SARS-CoV-2 in the absence of Zn (PDB 6W37) and Ncp7 of HIV-1 in the presence of Zn (Morellet et al., 1998) (PDB 1ESK), will be the basis to model BST2 disulfide bond plasticity induced by modulation of orf7a/orf8 Zn binding.

The resulting predicted structures will also be useful for the forthcoming experimental studies aimed at validating (or disproving) the function of orf7a/orf8 proteins as diversion tools of the interferon-dependent antiviral response.

### DATA AVAILABILITY STATEMENT

The raw data supporting the conclusions of this article will be made available by the authors, without undue reservation, to any qualified researcher.

### AUTHOR CONTRIBUTIONS

All authors listed have made a substantial, direct and intellectual contribution to the work, and approved it for publication.

### ACKNOWLEDGMENTS

We acknowledge the project MIUR-PRIN-201744NR8S Integrative tools for defining the molecular basis of the diseases: Computational and Experimental methods for Protein Variant Interpretation.

### REFERENCES

- Bonifacino, J. S., and Glick, B. S. (2004). The mechanisms of vesicle budding and fusion. *Cell* 116, 153–166. doi: 10.1016/S0092-8674(03)01079-1
- Chasapis, C. T. (2018). Interactions between metal binding viral proteins and human targets as revealed by network-based bioinformatics. *J. Inorg. Biochem.* 186, 157–161. doi: 10.1016/j.jinorgbio.2018.06.012
- Chaturvedi, U. C., and Shrivastava, R. (2005). Interaction of viral proteins with metal ions: role in maintaining the structure and functions of viruses. *FEMS Immun. Med. Microbiol.* 43, 105–114. doi: 10.1016/j.femsim.2004.11.004
- Coffin, J. M., Hughes, S. H., and E., V. H. (eds.). (1997). *Retroviruses*. Cold Spring Harbor, NY: Cold Spring Harbor Laboratory Press.
- Elstner, M., Porezag, D., Jungnickel, G., Elsner, J., Haugk, M., Frauenheim, T., et al. (1998). Self-consistent-charge density-functional tight-binding method for simulations of complex materials properties. *Phys. Rev. B* 58, 7260–7268. doi: 10.1103/PhysRevB.58.7260
- Furlan, S., La Penna, G., and Perico, A. (2008). Modeling the free energy of polypeptides in different environments. *Macromolecules* 41, 2938–2948. doi: 10.1021/ma7022155
- Gammoh, N. Z., and Rink, L. (2017). Zinc in infection and inflammation. *Nutrients* 9, 624–637. doi: 10.3390/nu9060624
- Gati, C., Stetsenko, A., Slotboom, D. J., Scheres, S. H., and Guskov, A. (2017). The structural basis of proton driven zinc transport by ZNTB. *Nat. Commun.* 8, 1–8. doi: 10.1038/s41467-017-01483-7
- Gordon, D. E., Jang, G. M., Bouhaddou, M., Xu, J., Obernier, K., White, K. M., et al. (2020). A SARS-CoV-2 protein interaction map reveals targets for drug repurposing. *Nature* 583, 459–468. doi: 10.1038/s41586-020-2286-9
- Guo, J., Wu, T., Anderson, J., Kane, B. F., Johnson, D. G., Gorelick, R. J., et al. (2000). Zinc finger structures in the human immunodeficiency virus type 1 nucleocapsid protein facilitate efficient minus- and plus-strand transfer. *J. Virol.* 74, 8980–8988. doi: 10.1128/JVI.74.19.8980-8988.2000
- Hourahine, B., Aradi, B., Blum, V., Bonafé, F., Buccheri, A., Camacho, C., et al. (2020). DFTB+, a software package for efficient approximate density functional theory based atomistic simulations. *J. Chem. Phys.* 152, 124101–124120. doi: 10.1063/1.5143190
- Humphrey, W., Dalke, A., and Schulten, K. (1996). VMD visual molecular dynamics. *J. Mol. Graph.* 14, 33–38. doi: 10.1016/0263-7855(96)0018-5
- Jorgensen, W. L., Chandrasekhar, J., Madura, J. D., Impey, R. W., and Klein, M. J. (1983). Comparison of simple potential functions for simulating liquid water. *J. Chem. Phys.* 79, 926–935. doi: 10.1063/1.445869
- Kirchdoerfer, R. N., and Ward, A. B. (2019). Structure of the SARS-CoV nsp12 polymerase bound to nsp7 and nsp8 co-factors. *Nat. Commun.* 10:2342. doi: 10.1038/s41467-019-10280-3
- Kluska, K., Peris-Díaz, M. D., Plonka, D., Moysa, A., Dadlez, M., Deniaud, A., et al. (2020). Formation of highly stable multinuclear  $ag_n s_n$  clusters in zinc fingers disrupts their structure and function. *Chem. Commun.* 56, 1329–1332. doi: 10.1039/C9CC09418K
- La Penna, G., Morante, S., Perico, A., and Rossi, G. C. (2004). Designing generalized statistical ensembles for numerical simulations of biopolymers. *J. Chem. Phys.* 121, 10725–10741. doi: 10.1063/1.1795694
- Le Tortorec, A., Willey, S., and Neil, S. J. D. (2011). Antiviral inhibition of enveloped virus release by tetherin/bst-2: action and counteraction. *Viruses* 3, 520–540. doi: 10.3390/v3050520

- Li, P., and Merz, K. M. (2017). Metal ion modeling using classical mechanics. *Chem. Rev.* 117, 1564–1686. doi: 10.1021/acs.chemrev.6b00440
- Maier, J. A., Martinez, C., Kasavajhala, K., Wickstrom, L., Hauser, K. E., and Simmerling, C. (2015). ff14SB: Improving the accuracy of protein side chain and backbone parameters from ff99SB. *J. Chem. Theory Comput.* 11, 3696–3713. doi: 10.1021/acs.jctc.5b00255
- Makov, G., and Payne, M. C. (1995). Periodic boundary conditions in ab initio calculations. *Phys. Rev. B* 51:4014. doi: 10.1103/PhysRevB.51.4014
- Moreira, N. H., Dolgonos, G., Aradi, B., da Rosa, A. L., and Frauenheim, T. (2009). Toward an accurate density-functional tight-binding description of zinc-containing compounds. *J. Chem. Theory Comput.* 5, 605–614. doi: 10.1021/ct800455a
- Morellet, N., Déméné, H., Teilleux, V., Huynh-Dinh, T., de Rocquigny, H., Fournié-Zaluski, M.-C., et al. (1998). Structure of the complex between the HIV-1 nucleocapsid protein NCp7 and the single-stranded pentanucleotide d(ACGCC). *J. Mol. Biol.* 283, 419–434. doi: 10.1006/jmbi.1998.2098
- Pang, Y.-P. (2001). Successful molecular dynamics simulation of two zinc complexes bridged by a hydroxide in phosphotriesterase using the cationic dummy atom method. *Proteins* 45, 183–189. doi: 10.1002/prot.1138
- Plimpton, S. (1995). Fast parallel algorithms for short-range molecular dynamics. *J. Comput. Phys.* 117, 1–19. doi: 10.1006/jcph.1995.1039
- Raffa, D. F., Rickard, G. A., and Rauk, A. (2007). *Ab initio* modelling of the structure and redox behaviour of copper(i) bound to a his-his model peptide: Relevance to the  $\beta$ -amyloid peptide of Alzheimer's disease. *J. Biol. Inorg. Chem.* 12, 147–164. doi: 10.1007/s00775-006-0175-9
- Swiecki, M., Omattage, N. S., and Brett, T. J. (2013). Bst-2/tetherin: structural biology, viral antagonism, and immunobiology of a potent host antiviral factor. *Mol. Immunol.* 54, 132–139. doi: 10.1016/j.molimm.2012.11.008
- Taylor, J. K., Coleman, C. M., Postel, S., Sisk, J. M., Bernbaum, J. G., Venkataraman, T., et al. (2015). Severe acute respiratory syndrome coronavirus ORF7A inhibits bone marrow stromal antigen 2 virion tethering through a novel mechanism of glycosylation interference. *J. Virol.* 89, 11820–11833. doi: 10.1128/JVI.02274-15
- te Velthuis, A. J. W., van den Worm, S. H. E., Sims, A. C., Baric, R. S., Snijder, E. J., and van Hemert, M. J. (2010). Zn<sup>2+</sup> inhibits coronavirus and arterivirus RNA polymerase activity *in vitro* and zinc ionophores block the replication of these viruses in cell culture. *PLoS Pathog.* 6:e1001176. doi: 10.1371/journal.ppat.1001176
- Tochio, N., Umehara, T., Nakabayashi, K., Yoneyama, M., Tsuda, K., Shirouzu, M., et al. (2015). Solution structures of the DNA-binding domains of immune-related zinc-finger protein ZFAT. *J. Struct. Funct. Genom.* 16, 55–65. doi: 10.1007/s10969-015-9196-3
- Vasilenko, N., Moshynskyy, I., and Zakhartchouk, A. (2010). SARS coronavirus protein 7a interacts with human Ap4A-hydrolase. *Virology* 7, 31–36. doi: 10.1186/1743-422X-7-31
- Wolf, D., Koblinski, P., Phillpot, S. R., and Eggebrecht, J. (1999). Exact method for the simulation of coulombic systems spherically truncated, pairwise R-1 summation. *J. Chem. Phys.* 110, 8254–8282. doi: 10.1063/1.478738
- Wu, A., Peng, Y., Huang, B., Ding, X., Wang, X., Niu, P., et al. (2020). Genome composition and divergence of the novel coronavirus (2019-nCoV) originating in china. *Cell Host Microbe* 27, 325–328. doi: 10.1016/j.chom.2020.02.001
- Wu, C., Liu, Y., Yang, Y., Zhang, P., Zhong, W., Wang, Y., et al. (2020). Analysis of therapeutic targets for SARS-CoV-2 and discovery of potential drugs by computational methods. *Acta Pharm. Sin. B.* 10, 766–788. doi: 10.1016/j.apsb.2020.02.008
- Xu, J., Zhao, S., Teng, T., Abdalla, A. E., Zhu, W., Xie, L., et al. (2020). Systematic comparison of two animal-to-human transmitted human coronaviruses: SARS-CoV-2 and SARS-CoV. *Viruses* 12:244. doi: 10.3390/v12020244
- Zhang, J., Yang, W., Piquemal, J.-P., and Ren, P. (2012). Modeling structural coordination and ligand binding in zinc proteins with a polarizable potential. *J. Chem. Theory Comput.* 8, 1314–1324. doi: 10.1021/ct200812y

**Conflict of Interest:** The authors declare that the research was conducted in the absence of any commercial or financial relationships that could be construed as a potential conflict of interest.

Copyright © 2020 Morante, La Penna, Rossi and Stellato. This is an open-access article distributed under the terms of the Creative Commons Attribution License (CC BY). The use, distribution or reproduction in other forums is permitted, provided the original author(s) and the copyright owner(s) are credited and that the original publication in this journal is cited, in accordance with accepted academic practice. No use, distribution or reproduction is permitted which does not comply with these terms.